Molecular recognition of *S*-nitrosothiol substrate by its cognate protein denitrosylase

Received for publication, July 18, 2018, and in revised form, December 5, 2018 Published, Papers in Press, December 11, 2018, DOI 10.1074/jbc.RA118.004947

Colin T. Stomberski[‡§1], Hua-Lin Zhou[‡], Liwen Wang[¶], Focco van den Akker[§], and Jonathan S. Stamler[‡‖2]**

From the [‡]Institute for Transformative Molecular Medicine, [§]Departments of Biochemistry and [‖]Medicine, and [¶]Center for Proteomics and Bioinformatics, Department of Nutrition, Case Western Reserve University, Cleveland, Ohio 44106 and the [**]Harrington Discovery Institute, University Hospitals Cleveland Medical Center, Cleveland, Ohio 44106

Edited by Ruma Banerjee

Protein *S*-nitrosylation mediates a large part of nitric oxide's influence on cellular function by providing a fundamental mechanism to control protein function across different species and cell types. At steady state, cellular *S*-nitrosylation reflects dynamic equilibria between *S*-nitrosothiols (SNOs) in proteins and small molecules (low-molecular-weight SNOs) whose levels are regulated by dedicated *S*-nitrosylases and denitrosylases. *S*-Nitroso-CoA (SNO-CoA) and its cognate denitrosylases, SNO-CoA reductases (SCoRs), are newly identified determinants of protein *S*-nitrosylation in both yeast and mammals. Because SNO-CoA is a minority species among potentially thousands of cellular SNOs, SCoRs must preferentially recognize this SNO substrate. However, little is known about the molecular mechanism by which cellular SNOs are recognized by their cognate enzymes. Using mammalian cells, molecular modeling, substrate-capture assays, and mutagenic analyses, we identified a single conserved surface Lys (Lys-127) residue as well as active-site interactions of the SNO group that mediate recognition of SNO-CoA by SCoR. Comparing SCoR^{K127A} *versus* SCoR^{WT} HEK293 cells, we identified a SNO-CoA–dependent nitrosoproteome, including numerous metabolic protein substrates. Finally, we discovered that the SNO-CoA/SCoR system has a role in mitochondrial metabolism. Collectively, our findings provide molecular insights into the basis of specificity in SNO-CoA–mediated metabolic signaling and suggest a role for SCoR-regulated *S*-nitrosylation in multiple metabolic processes.

S-Nitrosylation-mediated control of proteins, a fundamental mechanism for cellular regulation and signaling, operates across phylogeny and cell types. By current estimates, 70% of the proteome is subject to this modification (1, 2). Recent evidence indicates that *S*-nitrosylation is enzymatically regulated by protein *S*-nitrosylases (3) and denitrosylases (4). *S*-Nitrosylases operate as part of a multiprotein machinery (with NOSs and SNO synthases) for *S*-nitrosylation (5), analogous to the E1/E2/E3 ubiquitinylation machinery, and it is predicted that hundreds of nitrosylases mediate cellular NO signaling (5). By contrast, denitrosylases are likely fewer in number and fall into two categories: 1) direct protein denitrosylases, exemplified by thioredoxin-related proteins (6); and 2) low-molecular weight (LMW)[3] SNO reductases, including *S*-nitrosoglutathione (GSNO) reductases (7, 8) and *S*-nitroso-CoA (SNO-CoA) reductases (9). The latter group of enzymes carry out NAD(P)H-dependent reduction of GSNO or SNO-CoA, thereby regulating coupled equilibria between SNO-proteins and LMW-SNOs to control SNO-protein levels (10).

Two GSNORs and two SCoRs have been identified to date (10). In mammals, the primary SCoR is AKR1A1 (9), the founding member of the aldo-keto reductase superfamily of proteins (11). AKR1A1 has a preference for negatively charged carbonyl-containing substrates (12), including D-glucuronate, an intermediate in ascorbate synthesis in rodents (13). However, interestingly, the physiological substrates in humans are unknown and thus the primary functions of mammalian SCoR remain to be discovered. We recently demonstrated that SNO-CoA is in fact the likely preferred physiological substrate of SCoRs across phylogeny and that mammalian SCoR thereby regulates *S*-nitrosylation of proteins (9). Moreover, we have shown that SCoRs confer metabolic growth advantages in yeast (9) and reprogram cellular metabolism in mice to alleviate tissue injury (27). Thus, the SNO-CoA/SCoR system may play a newly discovered role in cellular metabolism.

The emerging paradigm wherein specificity in *S*-nitrosylation signaling derives, at least in part, from differential reactivities of LMW-SNOs, predicts a molecular basis for SNO recognition by LMW-SNO denitrosylases. However, structure-function relationships for LMW-SNO denitrosylases remain

This work was supported by National Institutes of Health Grants R01DK119506 (to J. S. S.), R01HL126900 (to J. S. S.), P01HL075443 (to J. S. S.), and P01HL128192 (to J. S. S.). The authors declare that they have no conflicts of interest with the contents of this article. The content is solely the responsibility of the authors and does not necessarily represent the official views of the National Institutes of Health.

This article contains Tables S1–S14, Figs. S1–S6, and Datasets S1–S3.

Proteomics data reported in this paper have been submitted to the PRIDE database under accession numbers PXD011880 and PXD011881.

[1] Supported in part by National Institutes of Health Grant T32GM007250.

[2] To whom correspondence should be addressed: Harrington Discovery Institute and Institute for Transformative Molecular Medicine, 10900 Euclid Ave. LC 7294, Cleveland, OH 44106. Tel.: 216-368-5724; E-mail: jonathan.stamler@case.edu.

[3] The abbreviations used are: LMW, low-molecular-weight; SNO, *S*-nitrosothiol; SNO-CoA, *S*-nitroso-coenzyme A; SCoR, SNO-CoA reductase; AKR1A1, aldo-keto reductase 1A1; iNOS, inducible nitric-oxide synthase; iTRAQ, isobaric tags for relative and absolute quantification; DETA-NONOate and DETA-NO, diethylenetriamine NONOate; LDHA, lactate dehydrogenase A; ENO1, α-enolase; FASN, fatty acid synthase; ACLY, ATP-citrate lyase; GAPDH, glyceraldehyde-3-phosphate dehydrogenase; OCR, oxygen consumption rate; ECAR, extracellular acidification rate; FCCP, carbonyl cyanide *p*-trifluoromethoxyphenylhydrazone; DTPA, diethylenetriaminepentaacetic acid; ACN, acetonitrile; ANOVA, analysis of variance.

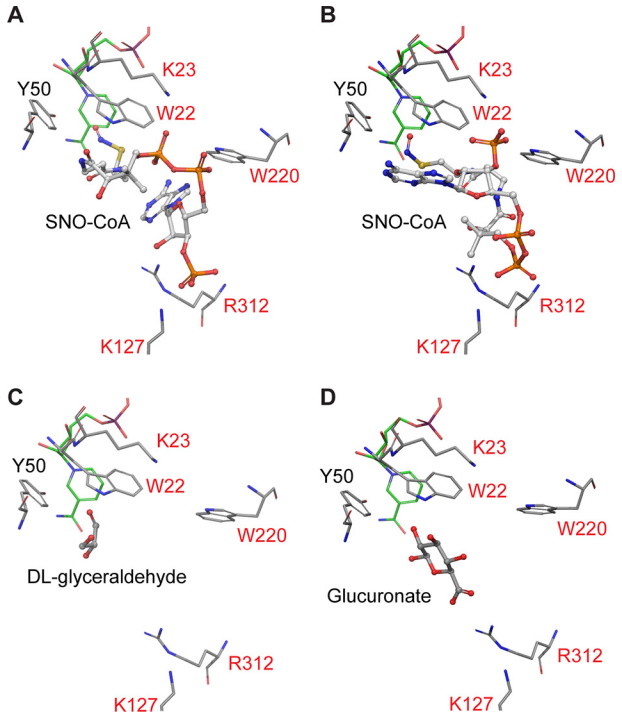

Figure 1. Molecular modeling of SNO-CoA within the SCoR active-site. *A–D,* models of SNO-CoA (in binding mode 1 (*A*) and binding mode 2 (*B*)), DL-glyceraldehyde (*C*), and glucuronate (*D*) bound to the SCoR active-site. Putative SCoR SNO-CoA interacting residues are labeled in *red*. NADPH carbons are colored *green*. Modeling was performed in Schrödinger Maestro and images were generated in PyMol.

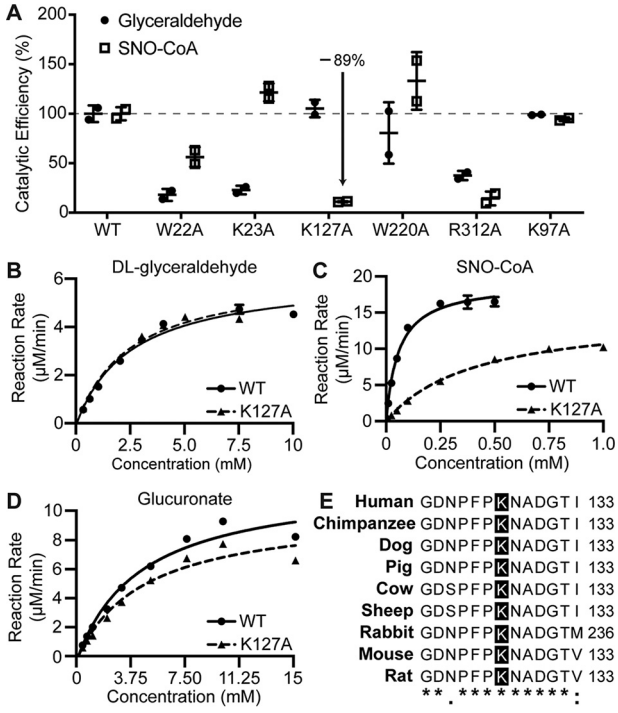

Figure 2. The conserved Lys-127 in SCoR facilitates SNO-CoA reductase activity. *A*, catalytic efficiency (K_{cat}/K_m) of SCoR mutants expressed relative to $SCoR^{WT}$. K_m and K_{cat} were determined from two independent purifications of $SCoR^{WT}$ and mutant enzymes, and used to generate an average catalytic efficiency for each enzyme and substrate. Scatter plot represents mean ± S.D. *B–D,* $SCoR^{K127A}$ inhibits SCoR-mediated SNO-CoA reduction. Michaelis-Menten curves for $SCoR^{WT}$ and $SCoR^{K127A}$ using DL-glyceraldehyde (*B*), SNO-CoA (*C*), and glucuronate (*D*) as substrates. Enzyme assays were performed in triplicate. Error bars are not shown for data points where standard deviation is very small. *E,* Lys-127 is conserved across mammalian species. Amino acid sequence alignment for select mammalian species. Sequences from Uniprot were aligned using ClustalW. Lys-127 is highlighted with a *black box*. The residue number of the final amino acid is listed on the *right*. *Asterisk* (*) indicates complete residue conservation; *colon* (:) indicates conservation of amino acids with strongly similar properties; *dot* (.) indicates conservation of amino acids with weakly similar properties.

largely unexplored. Thus, there is a general lack of understanding of how denitrosylases recognize their substrates within the cellular milieu. In particular, it remains unclear if these interactions depend on the R groups in RSNOs (*e.g.* GSH or CoA) and/or whether proteins may recognize the SNO moiety. Here we use molecular modeling and mutagenic analyses to determine the molecular mechanisms by which SCoRs bind and metabolize SNO-CoA. We then utilize mutant SCoR that is unable to bind SNO-CoA to identify novel targets of SNO-CoA–mediated *S*-nitrosylation in cellular systems, and to assess the role of SCoR in mitochondrial metabolism.

Results

Molecular modeling of SCoR-based specificity

To understand how SCoR recognizes SNO-CoA, we performed molecular modeling of SNO-CoA and the SCoR (AKR1A1) active-site to identify amino acids potentially mediating the SCoR–SNO-CoA interaction. Docking of SNO-CoA to the SCoR active-site produced two possible binding modes (Fig. 1, *A* and *B*) with the SNO group oriented toward NADPH and the catalytic Tyr-50 (14). Multiple charged or aromatic residues surrounding the SCoR active-site (Fig. 1, *A* and *B*, labeled in *red*) were predicted to either hydrogen bond with SNO-CoA or facilitate interaction of SCoR with SNO-CoA via van der Waals forces. Active-site binding modes for DL-glyceraldehyde and glucuronate were also obtained by docking calculations (Fig. 1, *C* and *D*). In accordance with previous work demonstrating a marked increase in K_m for glucuronate reduction upon mutation of Arg-312 (15), our model of glucuronate binding the SCoR active-site shows a strong interaction between the glucuronate carboxylic acid group and Arg-312, providing a level of confidence in our modeling results.

Essential role of $SCoR^{K127A}$ in SNO-CoA reductase activity

To test the role of the putative SNO-CoA–binding residues (Fig. 1, *red* amino acids) in mediating the SCoR–SNO-CoA interaction, we generated and purified recombinant (see "Experimental procedures") WT ($SCoR^{WT}$) and mutant SCoRs (Fig. S1) involving multiple putative substrate-interacting residues, and assessed the impact of these mutations on *in vitro* reduction of SNO-CoA and DL-glyceraldehyde. Mutations varyingly altered the catalytic efficiency (K_{cat}/K_m) of SCoR for both SNO-CoA and DL-glyceraldehyde (Fig. 2*A* and Table S1). Notably, $SCoR^{K127A}$ resulted in an ~90% reduction in SCoR catalytic efficiency for SNO-CoA with no effect on that of DL-glyceraldehyde (Fig. 2*A*). This selective reduction in catalytic efficiency was mediated primarily by an ~7-fold increase in K_m (with only a modest reduction in K_{cat}) (Fig. 2*C* and Table 1). $SCoR^{K127A}$ did not alter K_m or K_{cat} for DL-glyceraldehyde (Fig. 2*B* and Table 1) and only modestly reduced K_{cat} for glucuronate (Fig. 2*D* and Table 1). Diminished SNO-CoA turnover with

Table 1
Enzyme kinetics for SCoR/SCoR mutants with substrates

Substrate	Enzyme	K_m[a]	V_{max}[a]	K_{cat}[a]
		μM	μM/min	min^{-1}
SNO-CoA	WT	58 ± 4.4	19.2 ± 0.39	959
	K127A	410 ± 27	15.0 ± 0.41	750
	K127R	52 ± 4.6	14.6 ± 0.32	730
Dephospho-SNO-CoA	WT	49 ± 6.7	14.7 ± 0.53	733
SNO-cysteamine	WT	476 ± 72	2.45 ± 0.13	123
DL-glyceraldehyde	WT	2554 ± 260	6.14 ± 0.24	306
	K127A	2469 ± 256	6.24 ± 0.26	312
Glucuronate	WT	4555 ± 726	12.08 ± 0.78	604
	K127A	4728 ± 907	10.05 ± 0.26	502

[a] K_m and V_{max} were determined from Michaelis-Menten curves using GraphPad Prism 7. K_{cat} was calculated by dividing V_{max} by the enzyme concentration in each assay. Enzyme assays were performed in triplicate.

unaltered DL-glyceraldehyde reduction by $SCoR^{K127A}$ was confirmed by following NADPH consumption over 10 min (Fig. S2). Importantly, mutation of the active-site Tyr-50 abolished SCoR SNO-CoA reductase activity (Fig. S2), consistent with the previously identified role of Tyr-50 in the catalytic mechanism of SCoR (14) and indicating that SNO-CoA reduction by SCoR likely follows the canonical aldo-keto reductase catalytic mechanism, namely hydride transfer from NADPH and protonation by an active-site Tyr (14, 16).

Based on the crystal structure of SCoR, Lys-127 lies distant from the active-site (compared with other tested residues) and modeling does not predict an interaction of Lys-127 with either DL-glyceraldehyde or glucuronate (Fig. 1). Furthermore, mutation of Lys-97 (not shown in Fig. 1), which resides on the same surface as the SCoR active-site (although further away than Lys-127), does not alter SNO-CoA or DL-glyceraldehyde reduction by SCoR (Fig. 2*A* and Table S1). Importantly, Lys-127 is highly conserved among mammalian SCoRs (Fig. 2*E*), suggesting a key role for SCoR-regulated SNO-CoA signaling in mammals. These results demonstrate that among the tested substrates (including many previously studied substrates (14, 17, 18)), SNO-CoA is the kinetically preferred substrate for SCoR (Table 1), and that the conserved Lys-127 of SCoR mediates a specific enzyme–substrate interaction to facilitate SNO-CoA reduction.

SCoR recognizes the CoA backbone and SNO moiety in SNO-CoA

We next sought to determine how Lys-127 interacts with SNO-CoA to facilitate reduction by SCoR. One binding mode of SNO-CoA (Fig. 1*A*) predicted a hydrogen bond between Lys-127 and the 3′-phosphate of the 3′-phospho-ADP component of CoA; a second binding mode had the diphosphate linker of SNO-CoA interacting with Lys-127 (Fig. 1*B*). We hypothesized that if binding mode 1 is correct, $SCoR^{WT}$ would not effectively metabolize dephospho-SNO-CoA (SNO-CoA lacking the 3′-phosphate). However, reaction of dephospho-SNO-CoA with $SCoR^{WT}$ produced no change in K_m and only a modest reduction in K_{cat} (Fig. 3*A* and Table 1), indicating that this predicted hydrogen bond is not a primary driver of the interaction between SCoR and SNO-CoA (although it may affect turnover rate). Thus, it is more likely that Lys-127 interacts with the diphosphate linker in the CoA moiety of SNO-CoA, as predicted from binding mode 2 in Fig. 1*B*, where Lys-127 is ~3.0 Å from the CoA diphosphate and makes many favorable interactions with the CoA backbone.

The structure of the AKR superfamily is defined by a TIM barrel with interspersing loops, and variations in these loop regions provide specificity to the enzymes (12, 15). Lys-127 resides on a large loop between β-sheet 4 and α-helix 4 (of the TIM barrel), and provides a solvent-exposed positive charge (lost upon mutation to Ala) that could promote interaction of SNO-CoA with SCoR (Fig. S3, *A* and *B*). To test the requirement of a positively charged residue at this position, we substituted Lys-127 with Arg (Fig. S3*C*) and assessed the ability of $SCoR^{K127R}$ to metabolize SNO-CoA. Reaction of SNO-CoA with $SCoR^{K127R}$ produced no change in K_m and only a modest decrease in K_{cat} (Fig. 3*B* and Table 1). We further explored the requirement of a positive charge at residue 127 to facilitate the SNO-CoA–SCoR interaction by assessing the ability of $SCoR^{WT}$, $SCoR^{K127A}$, and $SCoR^{K127R}$ to bind bead-bound CoA and SNO-CoA. Both $SCoR^{WT}$ and $SCoR^{K127R}$, but not $SCoR^{K127A}$, efficiently bound CoA and SNO-CoA beads (Fig. 3, *C* and *D*). Together, these results demonstrate that a positively charged residue at position 127 is sufficient to drive the majority of the SCoR–SNO-CoA interaction, and that this interaction is mediated through the CoA moiety in SNO-CoA (likely through interaction with the diphosphate of the 3′-phospho-ADP component of CoA, as seen in Fig. 1*B*). Similar to the reaction of $SCoR^{WT}$ with dephospho-SNO-CoA, reaction of $SCoR^{K127R}$ with SNO-CoA modestly lowered K_{cat} (Table 1). Thus, the role of Lys-127 in SNO-CoA metabolism is likely 2-fold: (i) direct substrate recognition via the CoA diphosphate moiety and (ii) specific interaction between Lys-127 (as opposed to other positively charged residues) and the 3′-phosphate of CoA to facilitate optimal substrate turnover.

By contrast, two mutations ($SCoR^{K23A}$ and $SCoR^{W220A}$) increased SCoR catalytic efficiency for SNO-CoA by increasing K_{cat} without altering K_m (Fig. 2*A* and Table S1). These mutant enzymes also bound SNO-CoA beads as effectively as $SCoR^{WT}$ (Fig. S4, *A* and *B*), consistent with unaltered K_m values.

Notably, we also observed that $SCoR^{WT}$ bound SNO-CoA more effectively than CoA (Fig. 3, *C* and *E*), implying that SCoR interacts with the SNO moiety. Because the SNO group in SNO-CoA is part of cysteamine (Fig. 3*F*, top), we reasoned that SCoR might also metabolize SNO-cysteamine. Indeed, SCoR reduces SNO-cysteamine (Fig. 3*F*, *bottom*, and Table 1), albeit with a higher K_m and lower K_{cat} compared with SNO-CoA. Interestingly, the K_m of $SCoR^{WT}$ for SNO-cysteamine is similar to that of $SCoR^{K127A}$ for SNO-CoA (Table 1). These data point to the importance of the CoA moiety for effective SNO binding and turnover by SCoR.

As a further test of SCoR substrate recognition, we explored competitive inhibition of SNO-CoA reductase activity by CoA and acetyl-CoA (an alternative CoA derivative), finding both to be weak inhibitors (Fig. 3*G*). Using 100 μM SNO-CoA, CoA and acetyl-CoA exhibited IC_{50} values of 1.85 and 10.4 mM, respectively (Fig. 3*G*). Taken together, our results indicate that SCoR interacts with both the CoA and SNO moieties in SNO-CoA. Thus, SCoR preferentially acts on SNO-CoA and is unlikely to be inhibited by CoA or its derivatives at cytosolic concentra-

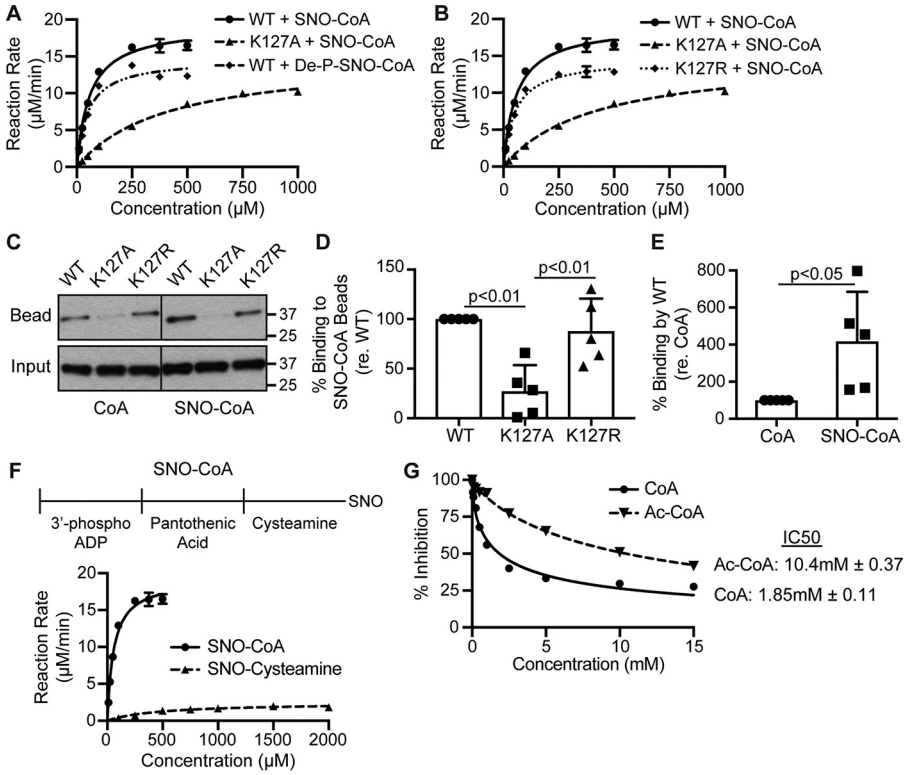

Figure 3. SCoR recognizes the CoA backbone and SNO moiety of SNO-CoA. *A,* dephosphorylated SNO-CoA alters V_{max} but not K_m. Michaelis-Menten curves for $SCoR^{WT}$ and $SCoR^{K127A}$ with SNO-CoA or dephospho-SNO-CoA (*De-P-SNO-CoA*) as substrates. Assays were performed in triplicate. Error bars are not shown for data points where standard deviation is very small. $SCoR^{WT}$ and $SCoR^{K127A}$ with SNO-CoA are from Fig. 2*C* and are shown here for comparison. *B,* $SCoR^{K127R}$ alters V_{max} but not K_m. Michaelis-Menten curves for $SCoR^{WT}$, $SCoR^{K127A}$, and $SCoR^{K127R}$ with SNO-CoA as substrate. Assays were performed in triplicate. Error bars are not shown for data points where standard deviation is very small. $SCoR^{WT}$ and $SCoR^{K127A}$ with SNO-CoA are from Fig. 2*C* and are shown here for comparison. *C,* $SCoR^{K127A}$ reduces binding to SNO-CoA and CoA. Representative Western blotting for SCoR following incubation of purified recombinant enzymes with SNO-CoA- or CoA-beads. *D,* quantification ($n = 5$) of $SCoR^{WT}$, $SCoR^{K127A}$, and $SCoR^{K127R}$ binding to SNO-CoA-beads from *C*. Bands were quantified using ImageJ. Scatter plot and *bars* represent mean ± S.D. p value < 0.01 by one-way ANOVA with Tukey's correction for multiple comparisons. *E,* SCoR preferentially binds SNO-CoA. Quantification ($n = 5$) of $SCoR^{WT}$ binding to SNO-CoA- or CoA-beads from *C*. Bands were quantified using ImageJ. *Scatter plot* and *bars* represent mean ± S.D. p value < 0.05 by Student's t test. *F,* SCoR metabolizes SNO-cysteamine. *Upper*, linear representation of the core components of SNO-CoA. *Lower*, Michaelis-Menten curves for WT SCoR and the substrates SNO-CoA and SNO-cysteamine. Assays were performed in triplicate. Error bars are not shown for data points where standard deviation is very small. $SCoR^{WT}$ with SNO-CoA is from Fig. 2*C* and is shown here for comparison. *G,* CoA and acetyl-CoA (*Ac-CoA*) poorly inhibit SNO-CoA reduction by SCoR. Increasing concentrations of CoA or Ac-CoA were added to a reaction mix of 100 μM SNO-CoA/NADPH and 20 nM $SCoR^{WT}$. Assays were performed in triplicate. Error bars are not shown for data points where standard deviation is very small. IC_{50} values were calculated in GraphPad Prism 7.

tions, allowing SCoR to serve its physiological function as a SNO-CoA reductase.

Identification of targets of SNO-CoA/SCoR-mediated S-nitrosylation/denitrosylation

Previous work (9) has identified numerous substrates of SCoR in yeast, whereas fewer mammalian substrates of SCoR have been identified (27). AKR1A1 constitutes ~90–95% of NADPH-dependent SNO-CoA reductase activity in murine kidney lysate (Fig. 4*A*), and addition of recombinant WT SCoR rescued NADPH-dependent SNO-CoA reductase activity in SCoR-null kidney lysate to a greater degree than recombinant $SCoR^{K127A}$ (Fig. 4*A*).

Utilizing the difference between $SCoR^{WT}$ and $SCoR^{K127A}$ activity, we sought to identify targets of SNO-CoA–mediated *S*-nitrosylation. SNO-CoA treatment of kidney lysate greatly enhanced whole cell protein *S*-nitrosylation, as visualized by Imperial staining following SNO-RAC (19) (Fig. 4*B*, *lanes 2* and *4*), and this increase was abrogated by the co-addition of NADPH to WT, and to a lesser degree SCoR-null, lysate (Fig. 4*B*, *lanes 3* and *5*). Addition of recombinant $SCoR^{WT}$, but not recombinant $SCoR^{K127A}$, to SCoR-deficient kidney lysate greatly reduced SNO-CoA-induced *S*-nitrosylation (Fig. 4*B*, *lanes 6* and *7*). SNO-proteins regulated by SCoR-dependent metabolism of SNO-CoA (Fig. 4*B*, *lanes 6* and *7*) were trypsin-digested and identified by isobaric tags for relative and absolute quantification (iTRAQ)-coupled LC-coupled tandem MS (LC-MS/MS) (Dataset S1), providing a genetically-validated list of mammalian targets of SNO-CoA–mediated *S*-nitrosylation.

To identify endogenous targets of SCoR-dependent denitrosylation we developed a tractable cellular model in HEK293 cells. We deleted endogenous SCoR utilizing the CRISPR/Cas9 system and stably overexpressed $SCoR^{WT}$, $SCoR^{Y50A}$ (catalytically dead), or $SCoR^{K127A}$ in SCoR-deficient cells (Fig. 5*A*; Fig. S5). Both $SCoR^{WT}$ and $SCoR^{K127A}$ (but not $SCoR^{Y50A}$) rescued SCoR-mediated DL-glyceraldehyde reduction (Fig. 5*B*, *top*); by contrast, only $SCoR^{WT}$ rescued SCoR–mediated SNO-CoA reduction (Fig. 5*B*, *bottom*). Following transient overexpression of iNOS (inducible nitric oxide synthase), SNO-proteins were enriched by SNO-RAC and identified by iTRAQ-coupled LC-MS/MS, and the nitrosoproteomes from $SCoR^{WT}$ and $SCoR^{K127A}$ stable cells were compared (Dataset S2). Notably, 50

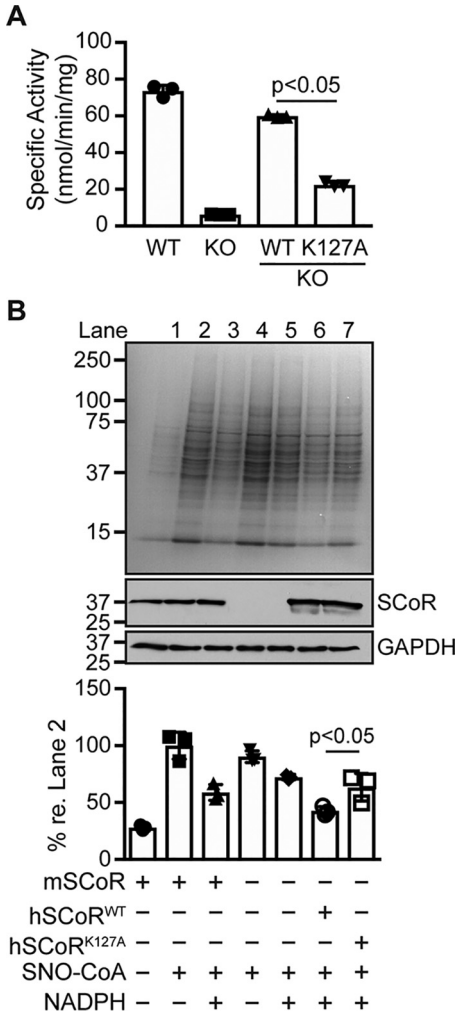

Figure 4. SCoR regulates SNO-CoA-dependent protein *S*-nitrosylation in tissue lysates. *A,* recombinant WT human SCoR rescues SNO-CoA reductase activity. SNO-CoA reductase specific activity was measured in kidney lysate from wildtype (*WT*) SCoR mice or SCoR knockout ($SCoR^{-/-}$; *KO*) mice ($n = 3$). Activity was reconstituted in $SCoR^{-/-}$ lysates by the addition of 150 nM recombinant human $SCoR^{WT}$ or $SCoR^{K127A}$. *Scatter plot* and *bars* represent mean ± S.D. *p* value < 0.05 by Student's *t* test. *B,* representative ($n = 3$) Imperial-stained SDS-PAGE gel showing SNO-proteins enriched by SNO-RAC. Mouse kidney lysates were treated with 50 μM SNO-CoA, 100 μM NADPH, and recombinant $SCoR^{WT}$ or $SCoR^{K127A}$ (as indicated) for 2 min. The *S*-nitrosylation reaction was stopped by the addition of acetone and SNO-RAC was performed. SCoR and GAPDH were assessed by Western blot analysis. Imperial-stained gels were quantified using ImageJ. *Scatter plot* and *bars* represent mean ± S.D. *p* value <0.05 by Student's *t* test for experimental *lanes 6* and *7*. *mSCoR*, endogenous mouse SCoR; *hSCoR*, recombinant human SCoR.

of the 123 SNO-proteins (~40%) identified as substrates of SCoR in HEK293 cells were also identified as targets of SNO-CoA in mouse kidney lysates (Dataset S3). Dataset S3 revealed overrepresentation of proteins involved in glycolysis, the tricarboxylic acid cycle, protein folding, and other cellular metabolic processes (Dataset S3).

We validated a top subset of putative targets of SCoR-dependent denitrosylation, including ubiquitin-like modifier-activating enzyme 1 (Ube1a/b), α-enolase (ENO1), lactate dehydrogenase A chain (LDHA), and fatty acid synthase (FASN). Analysis by SNO-RAC coupled to Western blotting demonstrated that $SCoR^{WT}$, but not $SCoR^{K127A}$ or $SCoR^{Y50A}$, lowered the levels of endogenous, iNOS-derived SNO-Ube1a/b, SNO-FASN, SNO-ENO1, and SNO-LDHA (Fig. 5*C*), identifying these proteins as targets of SNO-CoA–mediated (and SCoR-regulated) *S*-nitrosylation.

We also assessed whether reduced SNO-CoA binding by $SCoR^{K127A}$ would manifest in changes in *S*-nitrosylation by endogenous nitric oxide or with low concentrations of NO derived from the long half-life nitric oxide donor DETA-NONOate. Cells expressing $SCoR^{K127A}$ displayed enhanced basal *S*-nitrosylation of two CoA-dependent enzymes, SNO-FASN and SNO-ATP-citrate lyase (ACLY), and SNO-FASN and SNO-ACLY levels increased upon treatment with DETA-NONOate in $SCoR^{K127A}$, but not $SCoR^{WT}$, expressing cells (Fig. 5*D*). Additionally, SNO-Ube1a/b and SNO-pyruvate kinase M2 (a known SCoR target (27)) were basally elevated in $SCoR^{K127A}$ cells (Fig. 5*D*).

Furthermore, we evaluated SCoR activating mutations (K23A and W220A) to determine whether SCoR function is limited by enzyme turnover. Overexpression of $SCoR^{K23A}$ and $SCoR^{W220A}$ increased SNO-CoA reductase activity in cell lysates (Fig. S6, *A* and *B*), consistent with *in vitro* enzyme kinetics (Fig. 2*A* and Table 1). However, neither $SCoR^{K23A}$ nor $SCoR^{W220A}$ had added effect on SNO-FASN, SNO-ACLY, or SNO-GAPDH levels under basal conditions or in cells treated with DETA-NONOate (Fig. S6*C*), indicating that SCoR-mediated denitrosylation at baseline and under conditions of nitrosative stress is likely not limited by enzyme turnover. Taken together, our results suggest that SNO-CoA exists in equilibrium with myriad SNO-proteins across cellular processes to regulate protein *S*-nitrosylation, with SCoR controlling these equilibria via reduction of SNO-CoA.

SCoR regulates mitochondrial metabolism

We were interested to know if SCoR-mediated denitrosylation of proteins (Dataset S3) alters mitochondrial metabolism. Utilizing the Seahorse analyzer platform, we measured oxygen consumption rate (OCR, a measure of mitochondrial respiration) and extracellular acidification rate (ECAR, largely a measure of cellular glycolysis) in SCoR-KO cells stably expressing $SCoR^{WT}$ or $SCoR^{K127A}$. Cells expressing $SCoR^{K127A}$ displayed enhanced basal OCR (Fig. 6, *A* and *C*). Treatment with DETA-NONOate reduced OCR in both $SCoR^{K127A}$ and $SCoR^{WT}$ cells, potentially due to SCoR-independent inhibitory *S*-nitrosylation of respiratory chain components (20, 21). Both $SCoR^{K127A}$ and $SCoR^{WT}$ expressing cells increased OCR in response to cellular stress by oligomycin (ATP synthesis inhibitor) and FCCP (uncoupling agent). Basal ECAR was also slightly enhanced in $SCoR^{K127A}$ expressing cells (Fig. 6, *B* and *D*). DETA-NONOate treatment increased ECAR in both $SCoR^{WT}$ and $SCoR^{K127A}$ expressing cells, likely in response to reduced OCR. Although $SCoR^{WT}$ and $SCoR^{K127A}$ cells increased ECAR in response to oligomycin and FCCP, DETA-NONOate–treated cells were unable to increase ECAR. Taken together, these results suggest that increased *S*-nitrosylation by endogenous SNO-CoA increases mitochondrial respiration, and to a lesser degree glycolysis, whereas the effects of exogenous NO (to dramatically reduce mitochondrial respiration) are SCoR independent.

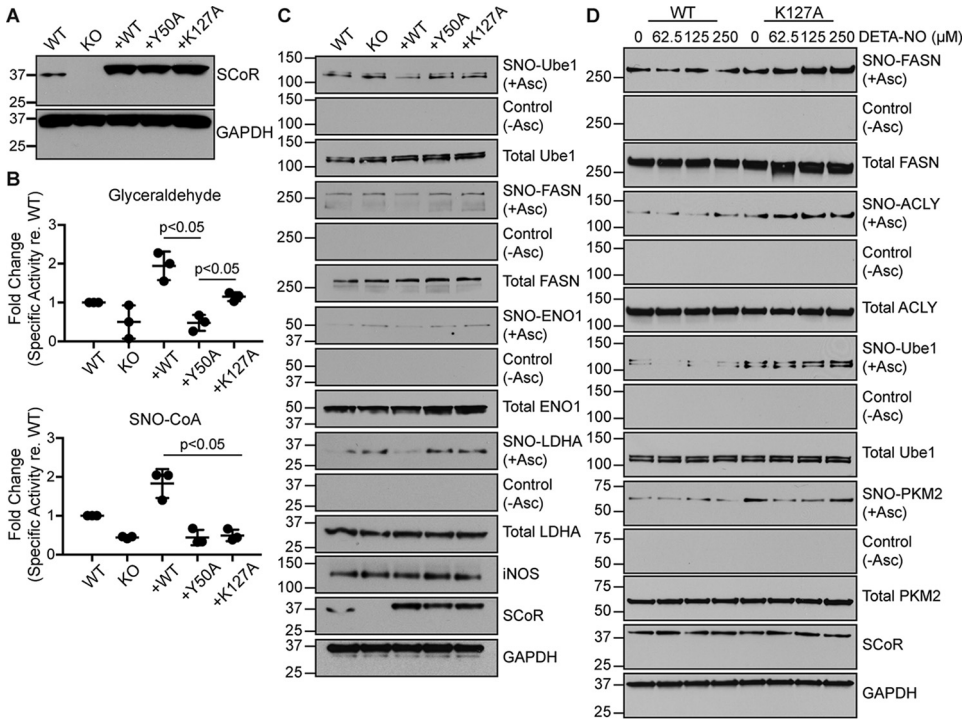

Figure 5. SCoR regulates endogenous protein *S*-nitrosylation. *A,* stable overexpression of SCoR in SCoR-knockout (*KO*) HEK293 cells. Representative Western blot analysis of SCoR expression in SCoR^{WT} cells, SCoR-KO cells, or KO cells stably expressing WT (+*WT*), SCoR^{Y50A} (+*Y50A*), or SCoR^{K127A} (+*K127A*). *B,* stable overexpression of SCoR^{WT} rescues SCoR-dependent SNO-CoA reductase activity in KO HEK293 cells. Fold-change in specific activity of DL-glyceraldehyde and SNO-CoA reducing activity in lysate from the indicated cell lines. Data represent the average fold-change in specific activity from 3 independent passages. Scatter plots represent mean ± S.D. *p* value <0.05 by Student's *t* test. *C,* SCoR regulates SNO-CoA-dependent protein *S*-nitrosylation. Western blot analysis of the *S*-nitrosylation status of putative targets of SCoR-mediated denitrosylation from Dataset S2. iNOS was overexpressed in the indicated cell lines for 24 h prior to cell harvest. SNO-proteins were enriched by SNO-RAC, separated by SDS-PAGE, and analyzed by Western blotting. *D,* Western blot analysis of the *S*-nitrosylation status of putative targets of SCoR-mediated denitrosylation. SCoR-KO HEK293 cells stably expressing SCoR^{WT} or SCoR^{K127A} were untreated or treated for 20 h with the indicated concentrations of DETA-NONOate (DETA-NO) prior to harvest for SNO-protein enrichment by SNO-RAC.

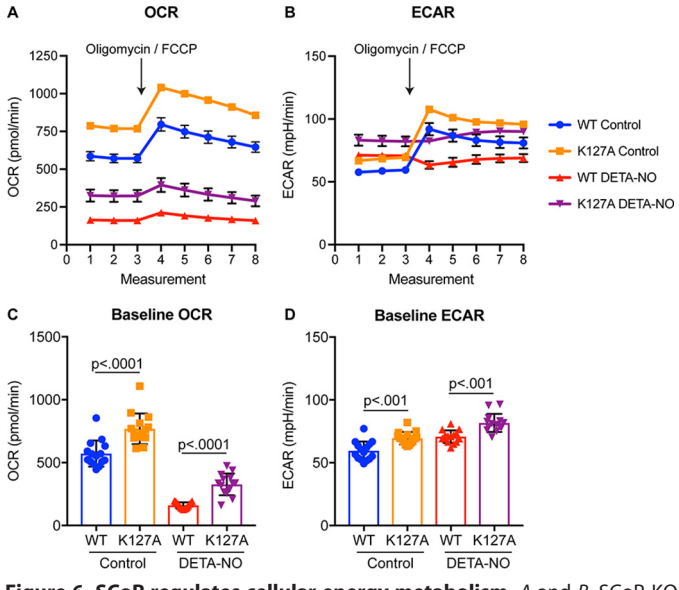

Figure 6. SCoR regulates cellular energy metabolism. *A* and *B,* SCoR-KO HEK293 cells stably expressing SCoR^{WT} or SCoR^{K127A} were assessed for OCR (*A*) and ECAR (*B*) using the Seahorse xFe24 analyzer. Cells were grown overnight and then treated with or without 125 μM DETA-NONOate (DETA-NO) for 20 h before analysis. Oligomycin (2 μM) and FCCP (3 μM) were co-injected following the 3rd measurement, as indicated by the *arrow*. Data represent mean ± S.E. of three independent replicates (with 5 data points each) per experimental group. Error bars are not shown for data points where mean ± S.E. is very small. *C* and *D* summarize data in *A* and *B*, respectively, before addition of oligomycin and FCCP. Data represent mean ± S.D. *p* value calculated by one-way ANOVA with Tukey's correction for multiple comparisons.

Discussion

Our structure/function studies on AKR1A1 provide the first molecular insights into recognition of a SNO substrate and strong support for the proposition that the enzyme's primary role is to regulate cellular *S*-nitrosylation. AKR1A1 is the founding member of the aldo-keto reductase family, and is highly conserved in mammals, yet a primary carbonyl substrate has not been identified in man (12). Our results (and previous studies (9, 14, 17, 18)) indicate that SNO-CoA is in fact a preferred endogenous AKR1A1 substrate and that AKR1A1 is the primary mammalian SNO-CoA reductase (SCoR). SNO-CoA recognition by SCoR involves interactions with both the CoA backbone (Lys-127) and the SNO moiety (active-site residues). The latter finding, *i.e.* recognition of the SNO group, has important consequences for the field as it represents a basis for specificity that has been heretofore missing from conceptual understanding of NO-based signaling. Knowledge that enzyme–RSNO interactions will likely entail molecular recognition of both R and SNO groups could also influence inhibitor design where SCoR inhibition proves beneficial.

Molecular recognition of the SNO group by SCoR is important for SCoR function *in situ*, as evidenced by preferential binding of SCoR to SNO-CoA *versus* CoA. Consequently, SCoR also catalyzes the reduction of SNO-cysteamine (Fig. 3*F*). But whereas the interaction of the SNO moiety with SCoR provides a mechanism to outcompete high levels of cellular CoA and CoA derivatives, interaction of the CoA moiety with Lys-127

will favor binding of SNO-CoA over SNO-cysteamine. Cytosolic concentrations of CoA are also likely to be much higher than cysteamine. Thus, reduction of SNO-cysteamine may be a fortuitous activity rather than a physiological function of the enzyme.

How exactly SCoR recognizes the SNO moiety is still unclear. The active-site of SCoR is comprised of four critical residues: proton-donating Tyr-50; Asp-45 and Lys-80, which influence both Tyr-50 pK_a and nucleotide binding (14); and His-113, which is important for substrate orientation (14). Notably, the active-site of SCoR is positively charged (Fig. S3), a characteristic that should markedly alter the electronic state of the SNO group through charge coordination with individual S–N–O atoms (10, 22). More specifically, the positively– charged residues near the active-site may draw electrons to the N or O (23), promoting interaction with His-113 to thereby orient SNO-CoA (and SNO-cysteamine) for efficient catalysis. This substrate orientation mechanism would be absent in CoA (or Ac-CoA). Interestingly, mutation of Arg-312 (a residue lining the active-site) to Ala greatly reduced SNO-CoA reductase activity through a primary effect on K_{cat}. This decrease in K_{cat} contrasts with the primary effect of Lys-127 mutation on K_m and may indicate importance of Arg-312 for SNO recognition and orientation. Collectively, these data suggest a catalytic sequence involving initial attraction of SNO-CoA to SCoR via CoA interaction with Lys-127 and subsequent polarization and orientation of the SNO moiety by Arg-312 and His-113. The reaction would be completed via hydride transfer from NADPH to the N atom of the S–N–O and protonation of the O atom by Tyr-50, similar to the conserved reaction mechanism for carbonyls (16).

The list of SNO-proteins regulated by SCoR includes overrepresentation in several metabolic processes, including glycolysis, TCA cycle, and amino acid metabolism (Dataset S3). This is supported by demonstration of altered cellular metabolic parameters, in particular mitochondrial parameters, in cells expressing mutant SCoR with impaired substrate (SNO-CoA) binding. Collectively, these data strengthen the case for an important physiological role for the SCoR/SNO-CoA system in NO-based cellular signaling and metabolism. Future work will determine the role of individual SNO-proteins in mediating metabolic effects and whether SCoR regulates whole-body metabolism in mammalian physiology and pathophysiology.

Interestingly, Lys-127 is a putative target of CoA-based acetylation and succinylation (24); either modification would neutralize the positive charge at that residue and thereby likely inhibit SCoR activity (similar to the K127A mutation). Consequently, Lys-127 may represent a locus for cross-talk between CoA-based post-translational modifications that could work in concert to regulate energy demands of the cell.

Experimental procedures

Animals

Animal studies were approved by the Institutional Care and Use Committee (IACUC) at Case Western Reserve University. All housing and procedures complied with the Guide for the Care and Use of Laboratory Animals (25) and the American Veterinary Medical Associations guidelines regarding euthanasia (26).

Molecular modeling

Static protein/flexible ligand modeling of the interaction of SNO-CoA, DL-glyceraldehyde, and glucuronate were performed using Maestro 9.9 software. The SCoR crystal structure (PDB code 3H4G) was prepared for docking by removing H_2O and fidarestat from the PDB file. In Maestro, original hydrogens were removed and replaced, bond orders were assigned, and the structure was minimized. A grid was prepared around the active site centered at $X = -2.0999$, $Y = -24.4072$, $Z = -6.5084$. CoA, DL-glyceraldehyde, and glucuronate structures were obtained from PubChem. The SNO-CoA structure was generated by editing the CoA structure in Maestro. All ligands were prepared for docking in Maestro using the ligand preparation function. Ligands were docked to the active-site grid using XP Glide Docking with post-docking minimization.

Generation and expression of recombinant WT and mutant SCoR

The human SCoR coding sequence was previously cloned into a pET21b vector (9). Human SCoR mutants were generated by site-directed mutagenesis of pET21b-SCoR using the Agilent QuikChange XL II system per the manufacturer's instructions. Mutants were verified by sequencing. Primers for specific mutations are listed in supporting Table S2. pET21b-SCoR and mutants were transformed into Rosetta2(DE3)pLysS *Escherichia coli* (EMD Millipore) and expression was induced by the addition of 100 μM isopropyl β-D-1-thiogalactopyranoside (Sigma) at $A_{600\,nm} = 0.4$. Bacteria were grown for 4 h at 25 °C and recombinant His-tagged SCoR was purified as previously described (9). Purification was assessed by SDS-PAGE followed by Imperial Protein Stain (Thermo Fisher).

Kinetic analysis of recombinant SCoR

Kinetic parameters of recombinant WT and mutant SCoR were determined in 50 mM phosphate buffer, pH 7.0, containing 100 μM EDTA (Sigma) and 100 μM DTPA (Sigma). Triplicate reactions were performed with 20 nM recombinant SCoR, 100 μM NADPH (Sigma), and varying concentrations of SNO-CoA, dephospho-SNO-CoA, SNO-cysteamine, DL-glyceraldehyde (Sigma), or D-glucuronate (Sigma). SNO-CoA, dephospho-SNO-CoA, and SNO-cysteamine were prepared by reacting equal volumes of 0.1 M CoA (Sigma), dephospho-CoA (Sigma), or cysteamine (Sigma) in 1 M HCl and 0.1 M $NaNO_2$ (Fluka Chemicals) in MilliQ water containing 100 μM EDTA and 100 μM DTPA. Initial rates were calculated using an absorbance decrease at 340 nm and an extinction coefficient of 7.06 mM^{-1} cm^{-1} (combined for SNO-CoA and NADPH). Kinetic parameters (K_m and V_{max}) were determined using GraphPad Prism 7, and K_{cat} was derived from V_{max} and enzyme concentration. For NADPH consumption curves, reactions (50 μM SNO-CoA or 3 mM DL-glyceraldehyde with 100 μM NADPH and 20 nM enzyme) were allowed to proceed for 10 min while measuring absorbance at 340 nm. CoA and Ac-CoA inhibition assays were performed in triplicate as above but with a static concentration of 100 μM SNO-CoA and varying concentrations of CoA and

Ac-CoA (Sigma) dissolved in 50 mM phosphate buffer, pH 7.0, containing 100 μM EDTA and 100 μM DTPA. IC_{50} was determined using GraphPad Prism 7.

CoA and SNO-CoA bead pulldown

CoA beads (50% slurry) were prepared by suspending CoA-agarose powder (Sigma) in water overnight at 4 °C. To generate SNO-CoA beads, CoA beads were washed twice with 30 volumes of 10 mM HCl and supernatant was aspirated. Pelleted CoA beads were resuspended in 0.5 ml of 10 mM HCl and 0.5 ml of 10 mM $NaNO_2$ was added to the suspension to generate SNO-CoA. Immediately following $NaNO_2$ addition, 10 ml of washing buffer (150 mM NaCl (Fisher), 1 mM EDTA, 1 mM DPTA, 0.1 mM neocuproine (Sigma) and 50 mM borate buffer, pH 8.2) was added into the tube to dilute SNO-CoA beads and the SNO-CoA beads were washed three times with washing buffer. For binding experiments, 1 μg of recombinant $SCoR^{WT}$, $SCoR^{K127A}$, or $SCoR^{K127R}$ was diluted in 1 ml of binding buffer (250 mM NaCl, 1 mM EDTA, 1 mM DPTA, 0.1 mM neocuproine, and 50 mM borate buffer, pH 8.2). 10 μl (10 ng) of protein solution was saved for input analysis. The remaining 990 μl of protein solution was incubated with 30 μl of 50% SNO-CoA or CoA beads for 2 h at 4 °C in the dark. After incubation, the beads were washed six times with binding buffer, and bound proteins were eluted with 50 μl of 1× SDS loading dye (Bio-Rad) containing 5% 2-mercaptoethanol (Sigma).

SCoR-dependent SNO-CoA reductase activity in mouse kidney lysate and analysis of protein S-nitrosylation

The generation of $SCoR^{-/-}$ mice was reported previously (7). Twelve-week-old male $SCoR^{+/+}$ (WT) and $SCoR^{-/-}$ mice were euthanized and tissue samples were collected and immediately frozen in liquid nitrogen. Kidney tissue was Dounce homogenized in 50 mM phosphate buffer, pH 7.0, containing 150 mM NaCl, 100 μM EDTA, 100 μM DPTA, and protease inhibitor mixture (Roche). Tissue extracts were cleared by centrifugation (two times at 20,000 × *g*, 30 min). Protein concentration was determined by bicinchoninic acid assay (Pierce). Assays for specific activity in kidney lysates were performed in 50 mM phosphate buffer, pH 7.0, containing 50 μM SNO-CoA, 100 μM NADPH, 100 μM EDTA, and 100 μM DPTA. Reactions were initiated by the addition of WT or $SCoR^{-/-}$ lysate (500 μg of protein) with or without 150 nM recombinant $SCoR^{WT}$ or $SCoR^{K127A}$ enzyme added to $SCoR^{-/-}$ lysate. The initial rate was calculated from the change in absorbance at 340 nm and an extinction coefficient of 7.06 mM^{-1} cm^{-1} (combined for SNO-CoA and NADPH). For SNO-protein analysis by SNO-RAC (18), similar reactions were performed using 500 μg/ml of protein with and without the addition of 100 μM NADPH, 50 μM SNO-CoA, and 150 nM recombinant enzyme, and allowed to proceed for 2 min. Reactions were stopped by the addition of 3 volumes of ice-cold acetone and proteins were incubated for 20 min at −20 °C. Precipitated proteins were pelleted by centrifugation (4,000 × *g* at 4 °C for 5 min). Following removal of supernatant, proteins were resuspended in HEN buffer, pH 8.0 (100 mM HEPES, 1 mM DTPA, 0.1 mM neocuproine) containing 2.5% SDS and 0.2% *S*-methyl methanethiosulfonate (Sigma) and incubated at 50 °C for 20 min with frequent vortexing. Proteins were again precipitated with 3 volumes of ice-cold acetone and incubated at −20 °C for 20 min. Precipitated proteins were pelleted by centrifugation and resuspended in 1 ml of HEN buffer containing 1% SDS. The process of precipitation and resuspension in 1 ml of HEN buffer with 1% SDS was repeated. Proteins were then incubated with thiopropyl-Sepharose beads (GE Healthcare) for 4 h in the dark with 30 mM ascorbate (Sigma). Beads were subsequently washed with HEN, 1% SDS buffer and 10-fold diluted HEN, 1% SDS buffer. Proteins were eluted from the beads in 1× SDS loading dye containing 10% 2-mercaptoethanol. Eluate was separated by SDS-PAGE and SNO-proteins were visualized with Imperial protein stain per the manufacturer's instructions.

Identification of SNO-proteins by iTRAQ-coupled LC-MS/MS

SNO-proteins enriched by SNO-RAC (previously described) were separated by SDS-PAGE and stained with Imperial protein stain. Each column of gel bands was sliced and collected in two 1.5-ml tubes. The gel slices were washed with 500 μl of 50% acetonitrile (ACN), 50% 100 mM ammonium bicarbonate for more than 5 h with vortexing. After removal of washing buffer, 400 μl of 100% ACN was added to gel pieces and vortexed for 10 min. After removal of ACN, gel pieces were dried in a speed vacuum dryer for 10 min. 200 μl of 10 mM dithiothreitol was added to dry gel pieces and vortexed for 45 min. 200 μl of 55 mM iodoacetamide was added to the gel pieces after removal of dithiothreitol buffer and incubated for 45 min in the dark. After removal of iodoacetamide buffer, gel pieces were washed with 400 μl of 1× iTRAQ dissolution solution, then 400 μl of ACN, and this cycle was repeated once. Gel pieces were dried for 10 min in a speed vacuum dryer. 500 ng of trypsin enzyme in 150 μl of 1× iTRAQ buffer was added to dried gel pieces on ice for 30 min, and then incubated overnight at 37 °C. Following incubation, the supernatant from digested protein solution was transferred to a 1.5-ml tube using gel-loading tips. 200 μl of extraction buffer of 60% ACN, 5% formic acid was added to gel pieces, vortexed for 30 min, and sonicated for 15 min. Supernatant containing peptide extracts was transferred to 1.5-ml tubes, and extraction was repeated two more times. The digested protein solution was dried completely. To label peptides with iTRAQ reagents, 30 μl of iTRAQ dissolution buffer (×10) were added to each sample tube (pH > 7.0). iTRAQ reagent (114, 115, 116, and 117) was brought to room temperature and 70 μl of ethanol was added to each reagent. One iTRAQ labeling reagent was added to each sample tube. The labeling reaction was allowed to proceed for more than 5 h at room temperature with vortexing. After labeling, the samples were mixed together and dried completely.

Prior to MS, samples were cleaned-up as follows. 160 μl of 5% ACN containing 0.5% trifluoroacetic acid (TFA) was added to the dried mixed-label sample. C18 ZipTips were wetted 5 times with 20 μl of 50% ACN and equilibrated with 100 μl of 5% ACN containing 0.5% TFA. Samples were then loaded to the tip by drawing and expelling 50 cycles to ensure complete binding. The tips were washed 10 times with 20 μl of 5% ACN containing 0.5% TFA. Peptides were eluted 3 times from tips with 20 μl of 60% ACN containing 0.1% formic acid, combined, and dried completely.

Digested peptides were separated by UPLC (Waters, Milford, MA) with a Nano-ACQUITY UPLC BEH300 C18. Separated peptides were continuously injected into an Orbitrap Elite hybrid mass spectrometer (Thermo Finnigan) by a nanospray emitter (10 μm, New Objective). A linear gradient was used in chromatography by using mobile phase A (0.1% formic acid in water) and B (100% ACN) at a flow rate of 0.3 μl/min. Chromatography started with 1% mobile phase B and gradually increased to 40% at 130 min, then increased to 90% within 2 min and stayed at 90% for 10 min to clean the column. All MS data were acquired in a positive ion mode. A full MS scan (m/z 300–1800) at 120,000 resolution was conducted; 10 MS2 scans (m/z 100–1600) were activated from five most intense peptide peaks of full MS scans. CID and HCD cleavage modes were performed alternatively on the same peptides selected from full MS scans. MS2 resolution of HCD is 15,000.

Bioinformatic software MassMatrix was used to search MS data against a database composed of sequences of mouse or human proteins (depending on origin of sample) from Uniprot and their reversed sequences were used as a decoy database. Modifications such as oxidation of methionine and labeling of cysteine (IA modifications) were selected as variable modifications in searching. For iTRAQ label searches, MS tagging of N terminus, Lys and/or Tyr were selected as variable modifications to test labeling efficiency and as fixed modifications for quantitative iTRAQ analysis. Trypsin was selected as an *in silico* enzyme to cleave proteins after Lys and Arg. Precursor ion searching was within 10 ppm mass accuracy, and product ions were within 0.8 Da for CID cleavage mode and 0.02 Da for HCD cleavage mode. 95% confidence interval was required for protein identification.

Generation of SCoR mammalian expression plasmid

The SCoR coding sequence was amplified from pet21b-SCoR with the following primers: F, 5′-GGGGACAAGTTTGTACAAAAAAGCAGGCTTCACCATGGCGGCTTCCTGTGTTCTA-3′; and R, 5′-GGGGACCACTTTGTACAAGAAAGCTGGGTTTCAGTACGGGTCATTAAAGGG-3′; or R, 5′-GGGGACCACTTTGTACAAGAAAGCTGGGTTGTACGGGTCATTAAAGGGGTA-3′ (to remove stop codon). The SCoR coding sequence was cloned into Gateway vector pDONR221 (Thermo Fisher) per the manufacturer's instructions and verified by sequencing. Mutant pDONR221-SCoR vectors were generated by site-directed mutagenesis using primers and procedures as described previously. Sequence-verified WT and mutant SCoR constructs were shuttled to pcDNA-DEST40 (Thermo Fisher) per the manufacturer's instructions and verified by sequencing.

Western blot analysis

Western blotting analyses were performed using standard methods. Antibodies used were: SCoR (Santa Cruz Biotechnology, sc-100500), GAPDH (Abcam, ab181602), FASN (Cell Signaling, 3180S), Ube1a/b (Cell Signaling, 4891S), ENO1 (Cell Signaling, 13410S), LDHA (Cell Signaling 3582S), ACLY (Cell Signaling, 13390), pyruvate kinase M2 (Santa Cruz Biotechnology, sc-365648), and NOS2 (Santa Cruz Biotechnology, sc-8310).

Assay of SCoR activity in cell lysate

HEK293 cells were purchased from the American Type Culture Collection (ATCC) and cultured at 37 °C, 5% CO_2 in growth media (DMEM (Gibco) supplemented with 10% fetal bovine serum (Sigma), and 1× antibiotic-antimycotic (Gibco)). Empty vector, WT, or mutant SCoR cDNA constructs were transfected into SCoR-WT or SCoR-KO HEK293 cells using Lipofectamine 2000 (Thermo Fisher) per the manufacturer's instructions. After 24 h, cells were washed 2 times with cold PBS and harvested in PBS with a cell scraper. Cells were pelleted at 1500 rpm for 3 min and supernatant was aspirated. Cells were resuspended in 50 mM phosphate buffer, pH 7.0, containing 100 μM EDTA, 100 μM DTPA, and protease inhibitor mixture (Roche). Cells were lysed by sonication and cell debris pelleted by centrifugation (20,000 × g at 4 °C for 15 min). The resulting supernatant was used for activity assays as described previously using 100 μM SNO-CoA or 3 mM DL-glyceraldehyde, 100 μM NADPH, and 25 μl of cell lysate. SCoR expression was verified by Western blot analysis.

Generation of SCoR-deficient HEK293 by CRISPR/Cas9

HEK293 cells were transfected with the Dharmacon Edit-R system to generate SCoR-deficient HEK293 cells, per the manufacturer's instructions. Briefly, HEK293 cells were transfected with a mixture of Cas9 plasmid, TracrRNA, and crRNA (targeting human SCoR; Dharmacon, CR-005087-05) using Dharmafect Duo (Dharmacon). After 24 h, cells were trypsinized and subcultured in growth media supplemented with 3.3 μg/ml of puromycin hydrochloride (Gibco). Cells were selected for 2 weeks with frequent media changes, and then single colonies were manually selected and individually plated for expansion. Loss of SCoR expression was verified by Western blot analysis.

Stable overexpression of SCoR

WT or mutant SCoR in pcDNA-DEST40 without a stop codon (or empty vector) was linearized using PvuI restriction enzyme (Thermo Fisher). WT or SCoR-deficient HEK293 cells were transfected with linearized constructs using Lipofectamine 2000 (Thermo Fisher) per the manufacturer's instructions. After 48 h, cells were trypsinized and subcultured in growth media supplemented with 500 μg/ml of Geneticin (Gibco). After several passages, SCoR expression was verified by Western blotting and SCoR activity was assessed as described previously.

Analysis of SNO-proteins in SCoR-deficient and -overexpressing HEK293 lines

SCoR-HEK cell lines were maintained in growth media supplemented with 500 μg/ml of Geneticin. For experiments using iNOS as the endogenous nitric oxide source, cells were transfected with human inducible nitric-oxide synthase in pcDNA-3.1 vector using Lipofectamine 2000 per the manufacturer's instructions. After 24 h, cells were washed with and harvested in cold PBS containing 100 μM EDTA and 100 μM DTPA. Cells were pelleted by centrifugation at 1500 rpm for 3 min. The supernatant was aspirated and cells were frozen in liquid nitrogen. For SNO-RAC analysis of SNO-proteins, cells

were thawed on ice and lysed by sonication in HEN buffer containing 1% Nonidet P-40 and 0.01% *S*-methyl methanethiosulfonate. Cell debris was pelleted by centrifugation (20,000 × *g* at 4 °C for 20 min) and the supernatant used for SNO-RAC analysis, as described previously. Proteins from replicates used for SNO-protein identification by MS were separated by SDS-PAGE and stained with Imperial protein stain, and gels were processed for MS as described above. Alternatively, SNO-proteins were visualized by Western blotting using standard methods and antibodies listed above.

For experiments using a nitric oxide donor, cells stably expressing $SCoR^{WT}$ or $SCoR^{K127A}$ were treated for 20 h with complete growth media containing the indicated concentrations of DETA-NONOate (Cayman Chemicals). DETA-NONOate was freshly prepared in 0.01 M NaOH and diluted in complete growth media to the final experimental concentration before addition to cells. SNO-proteins were enriched and analyzed by Western blotting as described in the previous paragraph. Alternatively, SCoR-KO cells were transfected with $SCoR^{WT}$, $SCoR^{K23A}$, or $SCoR^{W220A}$ for 6 h using PolyJet transfection reagent (SignaGen) per the manufacturer's instructions. After 6 h, transfection media was removed and replaced with fresh growth media with or without DETA-NONOate. After 20 h, cells were harvested for SNO-protein analysis as described above.

Metabolic analysis using Seahorse XFe24 analyzer

All assays were performed on the Agilent Seahorse XFe24 analyzer using the Cell Energy Phenotype Test Kit. XF24 microplates were coated with 5 μg/ml of poly-D-lysine (Corning) in water for 3 h. Poly-D-lysine was aspirated and plates were washed two times with Dulbeccco's PBS (Gibco). SCoR-KO cells stably expressing $SCoR^{WT}$ or $SCoR^{K127A}$ were trypsinized and resuspended in complete growth media to a concentration of 4×10^5 cells/ml. 100 μl of cell suspension was added to 10 wells per plate per cell line (40,000 cells per well). 250 μl of complete growth media was added to blank wells. Cells were allowed to settle and adhere for 5 h before 150 μl of complete growth media was added to cell wells for overnight growth.

After 24 h, 200 μl of media was removed from cell wells and replaced with 200 μl of fresh growth media with or without DETA-NONOate to a final concentration of 125 μM (5 wells per cell line were untreated; 5 wells per cell line were treated). Cells were incubated for another 20 h before analysis. Cell metabolic analysis was performed following the manufacturer's instructions. Briefly, assay medium was prepared as Agilent phenol red-free base medium supplemented with 10 mM glucose, 1 mM pyruvate, and 2 mM glutamine (all Agilent reagents). 200 μl of media was removed from all wells and wells were washed with 1 ml of assay medium. 450 μl of fresh assay media was added to each cell and blank well. Cells were incubated at 37 °C with room air for 1 h prior to analysis. XFe24 sensor cartridge was prepared as per the manufacturer's instructions. After a 1-h incubation, cells were analyzed using the default Cell Energy Phenotype program, injecting 2 μM oligomycin and 3 μM FCCP after the third measurement.

Author contributions—C. T. S., F. v. d. A., and J. S. S. conceptualization; C. T. S. data curation; C. T. S. formal analysis; C. T. S., H.-L. Z., and L. W. investigation; C. T. S. visualization; C. T. S., H.-L. Z., F. v. d. A., and J. S. S. methodology; C. T. S. writing-original draft; C. T. S. and J. S. S. writing-review and editing; J. S. S. supervision; J. S. S. funding acquisition.

Acknowledgments—We thank Precious McLaughlin and Alfred Hausladen for technical assistance.

References

1. Hess, D. T., Matsumoto, A., Kim, S.-O., Marshall, H. E., and Stamler, J. S. (2005) Protein *S*-nitrosylation: purview and parameters. *Nat. Rev. Mol. Cell Biol.* **6,** 150–166 CrossRef Medline
2. Abunimer, A., Smith, K., Wu, T.-J., Lam, P., Simonyan, V., and Mazumder, R. (2014) Single-nucleotide variations in cardiac arrhythmias: prospects for genomics and proteomics based biomarker discovery and diagnostics. *Genes (Basel)* **5,** 254–269 CrossRef
3. Anand, P., and Stamler, J. S. (2012) Enzymatic mechanisms regulating protein *S*-nitrosylation: implications in health and disease. *J. Mol. Med.* **90,** 233–244 CrossRef Medline
4. Benhar, M., Forrester, M. T., and Stamler, J. S. (2009) Protein denitrosylation: enzymatic mechanisms and cellular functions. *Nat. Rev. Mol. Cell Biol.* **10,** 721–732 CrossRef Medline
5. Seth, D., Hess, D. T., Hausladen, A., Wang, L., Wang, Y., and Stamler, J. S. (2018) A multiplex enzymatic machinery for cellular protein *S*-nitrosylation. *Mol. Cell.* **69,** 451–464.e6
6. Benhar, M. (2015) Nitric oxide and the thioredoxin system: a complex interplay in redox regulation. *Biochim. Biophys. Acta.* **1850,** 2476–2484 CrossRef Medline
7. Liu, L., Hausladen, A., Zeng, M., Que, L., Heitman, J., and Stamler, J. S. (2001) A metabolic enzyme for *S*-nitrosothiol conserved from bacteria to humans. *Nature* **410,** 490–494 CrossRef Medline
8. Bateman, R. L., Rauh, D., Tavshanjian, B., and Shokat, K. M. (2008) Human carbonyl reductase 1 is an *S*-nitrosoglutathione reductase. *J. Biol. Chem.* **283,** 35756–35762 CrossRef Medline
9. Anand, P., Hausladen, A., Wang, Y. J., Zhang, G. F., Stomberski, C., Brunengraber, H., Hess, D. T., and Stamler, J. S. (2014) Identification of *S*-nitroso-CoA reductases that regulate protein *S*-nitrosylation. *Proc. Natl. Acad. Sci. U.S.A.* **111,** 18572–18577 CrossRef Medline
10. Stomberski, C. T., Hess, D. T., and Stamler, J. S. (2018) Protein *S*-nitrosylation: determinants of specificity and enzymatic regulation of *S*-nitrosothiol-based signaling. *Antioxid. Redox Signal.* 10.1089/ars.2017.7403 CrossRef
11. Mindnich, R. D., and Penning, T. M. (2009) Aldo-keto reductase (AKR) superfamily: genomics and annotation. *Hum. Genomics* **3,** 362–370 Medline
12. Barski, O. A., Tipparaju, S. M., and Bhatnagar, A. (2008) The aldo-keto reductase superfamily and its role in drug metabolism and detoxification. *Drug Metab. Rev.* **40,** 553–624 CrossRef Medline
13. Gabbay, K. H., Bohren, K. M., Morello, R., Bertin, T., Liu, J., and Vogel, P. (2010) Ascorbate synthesis pathway: dual role of ascorbate in bone homeostasis. *J. Biol. Chem.* **285,** 19510–19520 CrossRef Medline
14. Barski, O. A., Gabbay, K. H., Grimshaw, C. E., and Bohren, K. M. (1995) Mechanism of human aldehyde reductase: characterization of the active site pocket. *Biochemistry* **34,** 11264–11275 CrossRef Medline
15. Barski, O. A., Gabbay, K. H., and Bohren, K. M. (1996) The C-terminal loop of aldehyde reductase determines the substrate and inhibitor specificity. *Biochemistry* **35,** 14276–14280 CrossRef Medline
16. Jin, Y., and Penning, T. M. (2007) Aldo-keto reductases and bioactivation/detoxication. *Annu. Rev. Pharmacol. Toxicol.* **47,** 263–292 CrossRef Medline
17. Branlant, G., and Biellmann, J. F. (1980) Purification and some properties of aldehyde reductases from pig liver. *Eur. J. Biochem.* **105,** 611–621 CrossRef Medline

18. Wermuth, B., Münch, J. D., and von Wartburg, J. P. (1977) Purification and properties of NADPH-dependent aldehyde reductase from human liver. *J. Biol. Chem.* **252,** 3821–3828 Medline
19. Forrester, M. T., Thompson, J. W., Foster, M. W., Nogueira, L., Moseley, M. A., and Stamler, J. S. (2009) Proteomic analysis of *S*-nitrosylation and denitrosylation by resin-assisted capture. *Nat. Biotechnol.* **27,** 557–559 CrossRef Medline
20. Brown, G. C., and Cooper, C. E. (1994) Nanomolar concentrations of nitric oxide reversibly inhibit synaptosomal respiration by competing with oxygen at cytochrome oxidase. *FEBS Lett.* **356,** 295–298 CrossRef Medline
21. Chouchani, E. T., Methner, C., Nadtochiy, S. M., Logan, A., Pell, V. R., Ding, S., James, A. M., Cochemé, H. M., Reinhold, J., Lilley, K. S., Partridge, L., Fearnley, I. M., Robinson, A. J., Hartley, R. C., Smith, R. A., Krieg, T., Brookes, P. S., and Murphy, M. P. (2013) Cardioprotection by S-nitrosation of a cysteine switch on mitochondrial complex I. *Nat. Med.* **19,** 753–759 Medline
22. Talipov, M. R., and Timerghazin, Q. K. (2013) Protein control of *S*-nitrosothiol reactivity: interplay of antagonistic resonance structures. *J. Phys. Chem. B* **117,** 1827–1837 CrossRef Medline
23. Timerghazin, Q. K., Peslherbe, G. H., and English, A. M. (2007) Resonance description of S-nitrosothiols: insights into reactivity. *Org. Lett.* **9,** 3049–3052 CrossRef Medline
24. Park, J., Chen, Y., Tishkoff, D. X., Peng, C., Tan, M., Dai, L., Xie, Z., Zhang, Y., Zwaans, B. M., Skinner, M. E., Lombard, D. B., and Zhao, Y. (2013) SIRT5-mediated lysine desuccinylation impacts diverse metabolic pathways. *Mol. Cell.* **50,** 919–930 CrossRef Medline
25. Committee for the Update of the Guide for the Care and Use of Laboratory Animals. (2011) *Guide for the Care and Use of Laboratory Animals*, National Academies Press, Washington, D.C., 10.17226/12910 Medline
26. AMVA Panel on Euthanasia. (2013) *AVMA Guidelines for the Euthanasia of Animals.* 2013 Edition, American Veterinary Medical Association, Schaumberg, IL
27. Zhou, H., Zhang, R., Anand, P., Stomberski, C. T., Qian, Z., Hausladen, A., Wang, L., Rhee, E. P., Parikh, S. M., Karumanchi, S. A., and Stamler, J. S. (2018) Metabolic reprogramming by the S-nitroso-CoA reductase system protects against kidney injury. *Nature* 10.1038/s41586-018-0749-z CrossRef Medline